GaInAsP/InP-based optical modulator consisting of gap-surface-plasmon-polariton waveguide: theoretical analysis

Tomohiro Amemiya,[1,*] Eijun Murai,[2] Zhichen Gu,[2] Nobuhiko Nishiyama,[2] and Shigehisa Arai[1,2]

[1]*Quantum Nanoelectronics Research Center, Tokyo Institute of Technology, 2-12-1 O-okayama, Meguro-ku, Tokyo 152-8552, Japan*
[2]*Department of Electrical and Electronic Engineering, Tokyo Institute of Technology, 2-12-1 O-okayama, Meguro-ku, Tokyo 152-8552, Japan*
**Corresponding author: amemiya.t.ab@m.titech.ac.jp*

Received July 7, 2014; revised September 21, 2014; accepted September 28, 2014; posted October 6, 2014 (Doc. ID 216529); published October 30, 2014

We propose a III–V-based electro-absorption plasmon modulator that can be used to construct fully monolithic plasmonic integrated circuits. Our device consists of a GaInAsP/InP gap-surface-plasmon-polariton waveguide with TiO_2/ITO layers on both sides of the InGaAsP core. Using this design, the intensity of transmitted light can be modulated by controlling the carrier concentration of the ITO layer, as a positive gate voltage induces electron accumulation in the ITO layer (this is similar to the operation of FinFETs). The extinction ratio was 4.5 dB/μm with a gate voltage swing of 0–5, and the insertion loss was found to be 1.5 dB/μm. The figure of merit (ratio of extinction ratio to transmission loss) is 3, a result that is far superior to other conventional Si-based plasmonic photomodulators.

OCIS codes: (130.0130) Integrated optics; (130.4110) Modulators; (250.5403) Plasmonics.
http://dx.doi.org/10.1364/JOSAB.31.002908

1. INTRODUCTION

Photonic integrated circuits (PICs) have made remarkable progress in the past few decades with the development of applications in the fields of optical communication, sensing, and imaging. At present, considerable attention is being paid to downscaling and reducing the power consumption of photonic devices to produce advanced PICs with high-density integration and high-level functionality.

The III–V compound PIC excels in functionality because it can monolithically integrate various photonic devices including light sources (lasers and light-emitting diodes), modulators, isolators, and detectors [1–3]. At the same time, the silicon PIC has been actively studied because it has the potential for ultrahigh-density integration that makes use of strong optical confinement, due to a large difference between the refractive indices of Si and SiO_2 [4–7]. However, it is still difficult to create monolithic light sources on silicon platforms because of the indirect bandgap of Si. Therefore, silicon PICs for practical use tend to take the form of hybrid integration with III–V compound devices [8–11].

Toward next-generation PICs, plasmonic integration technology based on surface plasmon polaritons has attracted growing attention in recent years [12–14]. Plasmonic integration has a considerable advantage in that it enables III–V compound photonic devices to be integrated into an extremely tiny size beyond the diffraction limit [15]. Using this technology will enable us to manufacture III–V compound PICs with high integration density, superior to that of silicon PICs. To further this goal, nanoscale III–V photonic devices based on the plasmonic integration concept are beginning to be developed: leading examples are ultralow threshold nanolasers [16–19] and high-speed, highly sensitive nanodetectors [20–22].

In this paper, we demonstrate the theoretical possibility of nanoscale III–V photonic modulators based on the plasmonic integration. Plasmonic integration technology has been applied to Si-based photonic modulators, and the production of several devices has been reported [23–26]. However, these Si-based devices are incompatible with monolithic integration including light sources. The large transmission loss caused by metal absorption in these devices is also an obstacle to practical use. The plasmonic III–V modulator we propose can overcome these problems to achieve both high modulation efficiency and low metal loss.

In the following sections, we first propose a III–V-based electro-absorption plasmon modulator. Our device consists of a plasmon-polariton waveguide in which the transmittance of light can be controlled by a gate voltage. We then confirm the operation of the device with the aid of computer simulation based on the finite element method. The simulation shows that an extinction ratio of 4.5 dB/μm can be obtained with a gate voltage swing of 5 V. The transmission loss, or insertion loss, is 1.5 dB/μm at a gate voltage of 0 V. Therefore, the figure of merit (ratio of extinction ratio to transmission loss) is 3, a result far superior to those of Si-based plasmonic photomodulators.

2. DEVICE STRUCTURE AND OPERATION PRINCIPLES

The modulator we propose consists of a gap-plasmon-polariton (GPP) waveguide with a gate to control the light transmittance.

Figure 1(a) gives a three-dimensional view of our device, while Fig. 1(b) is a cross section perpendicular to the light propagation. The core of the device is a waveguide consisting of an i-InGaAsP layer (bandgap wavelength = 1.22 μm) sandwiched between i-InP (upper) and n-InP (lower) clad layers. Both sides of the InGaAsP core are side-etched to form a deep-ridge waveguide and covered with a transparent conductive indium-tin-oxide (ITO) layer, a TiO_2 insulating layer, and a metal (Au with a Ti buffer) gate, in this order. We have designed the device to operate at a wavelength of 1550 nm. [A sample fabrication process for an actual physical device is as follows: (1) high mesa formation by dry etching, (2) wet etching on both sides of the InGaAsP core, (3) deposition of the ITO and TiO_2 with atomic layer deposition, and (4) metal electrode formation.]

In this device, the gap-surface-plasmon-polariton (GSPP) waves are excited along the interface of the gate metal and the TiO_2/ITO layers on both sides of the InGaAsP core. This produces strong optical confinement in the waveguide beyond the limit of diffraction. The polarization of the propagating light is transverse electric (TE), the same as for most existing PICs. This is a considerable advantage over other plasmon modulators [23–26], which are designed for transverse magnetic (TM) mode operation.

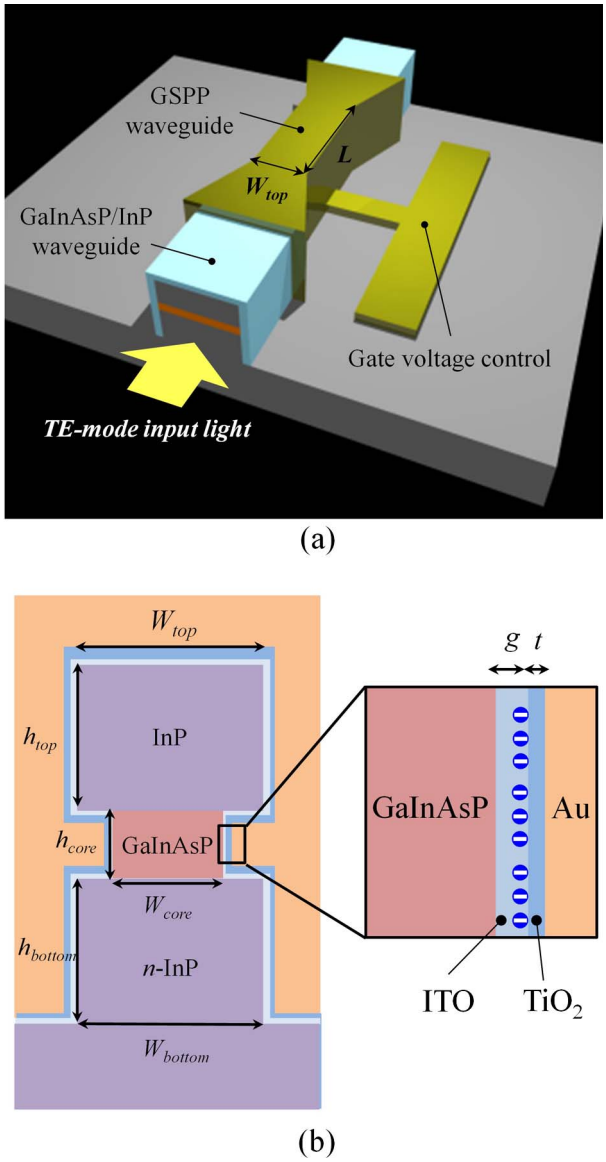

Fig. 1. (a) Schematic bird's-eye view image of GaInAsP/InP plasmon-polariton modulator with ITO thin film. (b) Schematic cross-section image of modulation region of device.

The intensity of transmitted light can then be modulated by controlling the carrier concentration of the ITO layer. Carrier control can be achieved by applying a voltage signal between the metal gate and the n-InP lower clad layer. A positive gate voltage induces electron accumulation in the ITO layer (this is similar to the operation of FinFETs). The peak position of the GPP-wave distribution occurs in the TiO_2/ITO layers, and therefore the light transmission can be modulated effectively as a result of the electron accumulation in the ITO layer.

The important indices of the modulators are the extinction ratio and insertion loss. In plasmon-polariton devices (including our device), metal parts strongly absorb light and reduce insertion loss. Therefore, reducing insertion loss is of particular concern.

3. MODULATING OPTICAL PROPERTIES OF ITO LAYER

To design the device, we determined the optical properties of ITO, i.e., the refractive index and absorption coefficient, as functions of carrier density.

The optical response of electrons in transparent conductive oxides such as ITO can be determined approximately using the Drude model and the Tauc–Lorentz model [27]. The plasma frequency, ω_p, and the relaxation coefficient, Γ, of the conductive oxide are given by

$$\omega_p(N) = \left(\frac{e^2 N}{m^*(N)\epsilon_\infty \epsilon_0}\right)^{\frac{1}{2}}, \tag{1}$$

$$\Gamma(N) = \frac{e}{m^*(N)\mu_{\text{opt}}}, \tag{2}$$

where N is the density of the electrons, e is the elementary charge, ϵ_0 is the vacuum permittivity, ϵ_∞ is the relative permittivity at optical frequencies, μ_{opt} is the electron mobility at optical frequencies, and $m^*(N)$ is the effective mass as a function of N. Note that N is the total density of the electrons, i.e., the sum of electrons from including both dopants and electrons induced by the gate-field effect. Taking the nonparabolicity and degeneracy of the conduction band into account [28–30], $m^*(N)$ is given by

$$m^*(N) = m_0^*\left[1 + \frac{2P\hbar^2}{m_0^*}(3\pi^2 N)^{\frac{2}{3}}\right]^{\frac{1}{2}}, \tag{3}$$

where m_0^* is the electron mass and P is a fitting parameter, equivalent to 0.18 eV^{-1} for ITO [31]. Here we set the electron mass m_0^* to be $0.4m_0$ considering the Moss–Burstein shift, because ITO is always degenerately doped.

Using Eqs. (1)–(3) and the parameters given in Table 1, we calculated the refractive index and absorption coefficient of ITO as a function of wavelength for various electron densities. The results are listed in Fig. 2. At the optical communication wavelength of 1.55 μm, both the refractive index and the

Table 1. Parameters Used in the Simulation

Material Parameters		
Parameter	Symbol	Value
Electron mass (degenerately doped ITO thin film)	m_0^*	0.4
Fitting parameter (ITO thin film)	P	0.18 eV^{-1}
Electron mobility at optical frequencies (ITO thin film)	μ_{opt}	25 cm^2/Vs
Relative permittivity at optical frequencies (ITO thin film)	ε_∞	3.8
Refractive indices of the III–V compound semiconductor	—	InP: 3.17 GaInAsP: 3.38
Refractive index of TiO_2	—	2.2
Refractive index of gold (Au)	—	0.145 + 10j

Structure Parameters		
Parameter	Symbol	Value
Height of InP top/bottom layer	$h_{top/bottom}$	400 nm
Width of InP top/bottom layer	$W_{top/bottom}$	500 nm
Height of GaInAsP core layer	h_{core}	200 nm
Width of GaInAsP core layer	W_{core}	Variable
Thickness of TiO_2 insulator	t	Variable
Thickness of ITO thin film	g	Variable

absorption coefficient change significantly with electron density. At low carrier densities (sufficiently lower than $5 \times 10^{20}/cm^3$), the ITO shows dielectric properties with very little light absorption. As the carrier density increases, however, the ITO changes from a dielectric to a metallic material and demonstrates strong light absorption. By utilizing this characteristic, we can create plasmon-polariton modulators with a large extinction ratio and low insertion loss.

The theoretical characteristic mentioned above is also applicable to other conditions as follows: (1) carrier concentration increased by doping in a material; (2) carriers induced by an external bias voltage. Therefore, the subsequent discussion is based on the results of this section.

4. DETERMINING TiO_2 THICKNESS AND ITO DOPANT DENSITY

We then designed a device prototype. The thickness of the InGaAsP core layer was set to 200 nm, and the thickness and width of the InP clad layers to 400 and 500 nm, respectively. Other important dimension parameters are the width of the core layer, the thicknesses of the TiO_2 and ITO layers, and the dopant density of the ITO layer. This section describes the determination of the optimal TiO_2 thickness and ITO dopant density.

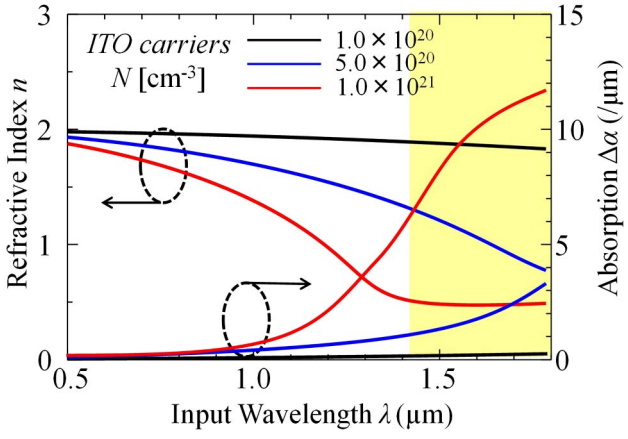

Fig. 2. Dependence of refractive index and absorption coefficient on wavelength, with carrier density as a parameter.

The TiO_2 thickness has a significant influence on the GSPP wave states. We simulated the propagation of light along the core for various values of TiO_2 thickness, and the finite difference method with the scattering boundary condition was then applied. The parameters used in this simulation are listed in Table 1.

Figure 3(a) depicts the optical confinement factor and propagation loss of light as a function of the core width, W_{core}, with the TiO_2 thickness as a parameter. In this simulation, we assumed a structure with no ITO layer; that is, we set the ITO thickness to 0. Figure 3(b) shows the distribution of the electric field strength of the GSPP waves excited in the waveguide. It is apparent that the hybrid-mode GSPP waves [32] are excited. With large TiO_2 thicknesses, the optical waves leak into the clad layers to produce a large propagation loss. With small thicknesses, effective optical confinement is established, and therefore propagation loss remains small, even if W_{core} is reduced beyond the diffraction limit. However, the TiO_2 thickness cannot be reduced without limit because this layer has to withstand the gate voltage. We therefore set it to 10 nm.

We then studied the effect of the electron density of the ITO layer on the light transmission loss. Figure 4 shows the results for light of 1.55 μm wavelength, with W_{core} as a parameter. In this example, we set the thickness of the ITO layer to 5 nm and used the data given in Fig. 2. At low electron densities (region A), the ITO behaves as a dielectric (see Fig. 2). In this condition, the GSPP waves are in the normal mode, and the distribution peak of the waves remains a small distance from the Au gate layer. This results in a small propagation loss. As the electron density increases (region B), the ITO changes from dielectric to metallic. In this condition, the GSPP waves transition into the strongly confined mode, and the distribution peak of the waves moves to the gate layer. As a result, the propagation loss abruptly increases due to absorption in the gate metal.

To operate the device as a modulator, a driving voltage is applied to the gate to change the electron density of the ITO layer. If the gate voltage is 0 V, the electron density is equal to the dopant density in the ITO. When a positive gate voltage is applied, the electron density increases because field-induced electron accumulation is added. To achieve small insertion loss, the operating point of the device must be in region A (see Fig. 4) at a gate voltage of 0 V. To achieve high modulation efficiency, the operating point must move deeply into region B at positive gate voltages. Considering the above, we set the dopant density to 1.0×10^{20} cm^{-3}.

5. SIMULATING MODULATOR OPERATION

We simulated the operation of the device and calculated the extinction ratio and insertion loss. To achieve this, we first calculated the carrier accumulation in the ITO layer induced by the gate voltage, using a device simulator (Silvaco ATLAS Device3D) comprising the Poisson equation, the electron and hole continuity equation, the parallel electric field-dependent

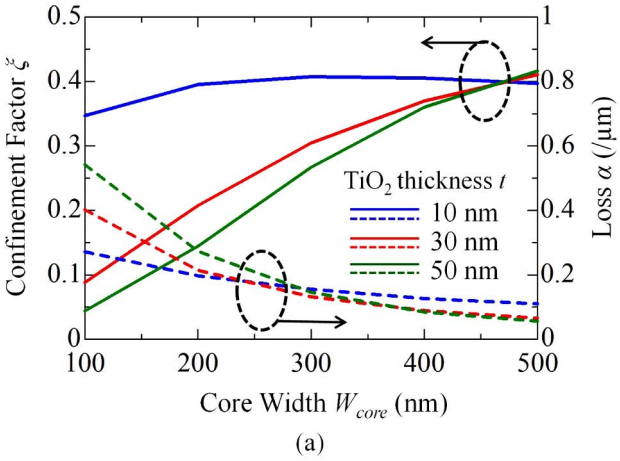

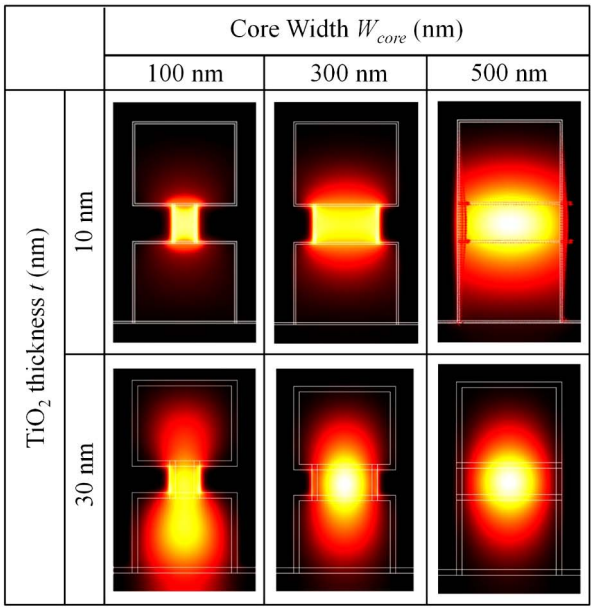

Fig. 3. (a) Calculated core confinement factor and propagation loss in GPP waveguides as a function of W_{core}, with TiO_2 film thickness, t, as a parameter. (b) Mode distribution profile in each structure.

mobility model, the concentration-dependent carrier mobility model, the Shockley–Read–Hall (SRH) recombination model, the material-dependent band parameter model, and Fermi–Dirac statistics. Figure 5 shows the electron distribution in the ITO layer for various gate voltages. In simulation, the TiO_2 and ITO thicknesses were set to 10 and 5 nm, respectively, and the dopant density in the ITO was 1×10^{20} cm^{-3}. The maximum driving voltage was set to 5 V to prevent the TiO_2 layer from breakdown. The resultant carrier accumulation occurred within 2 nm of the TiO_2/ITO interface. The carrier density at the interface increased to 6×10^{20} cm^{-3} for a gate voltage of 5 V, and the ITO changed its optical properties from dielectric to metallic. The width and density of the carrier accumulation depended only on the gate voltage and did not depend on the ITO thickness, provided the thickness was equal to or larger than 5 nm.

From the electron distribution in the ITO layer and the data given in Fig. 2, we determined the profile of the optical constant in the ITO layer. We then calculated the distribution

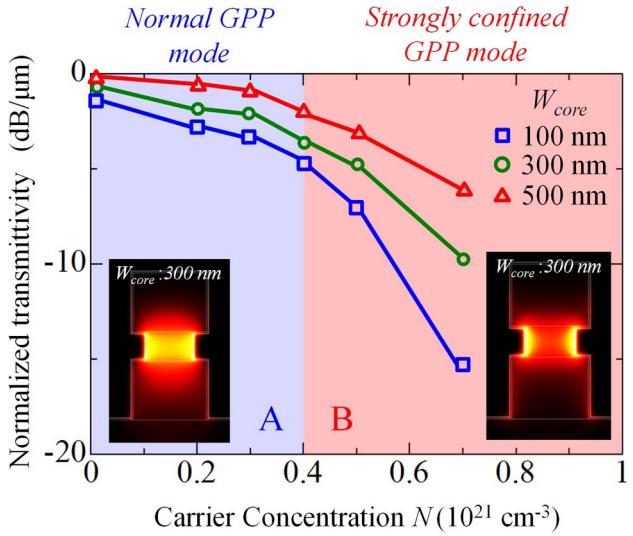

Fig. 4. Calculated propagation loss of GPP waveguide as a function of initial doping concentration in ITO thin film, with W_{core} as a parameter.

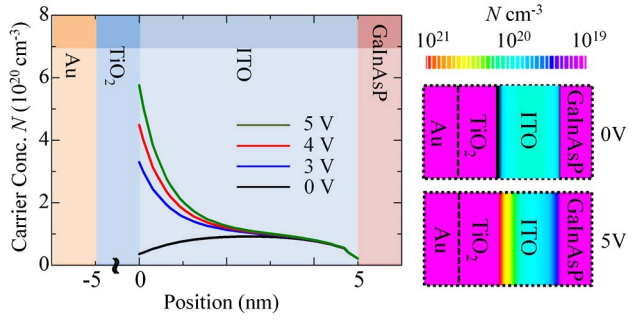

Fig. 5. Carrier concentration distribution near the TiO_2/ITO interface under bias voltage, with ITO film thickness of 5 nm.

of the GSPP waves in the device, using the finite element method. Figure 6 shows a sample result, where the InGaAsP core width is 100 nm, the TiO_2 thickness is 10 nm, and the dopant density of the ITO is 1×10^{20} cm^{-3}. As the gate voltage increases, the distribution profile of the light is drawn toward both sides of the waveguide because the ITO changes to a

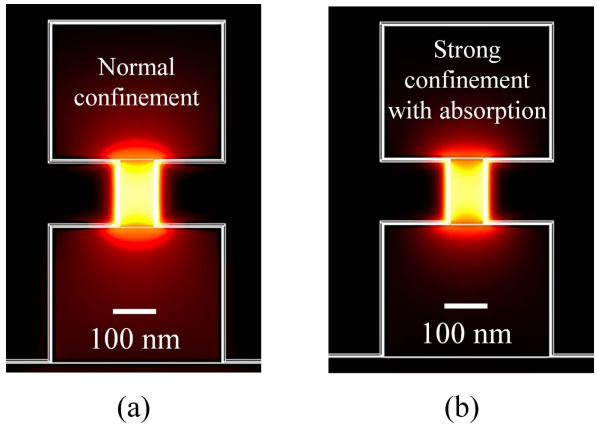

Fig. 6. Mode field distribution (a) without bias voltage and (b) with bias (5 V). The distribution profile of the light is pulled toward both sides of the waveguide because the ITO changes to a metallic state at the Al_2O_3/ITO interface.

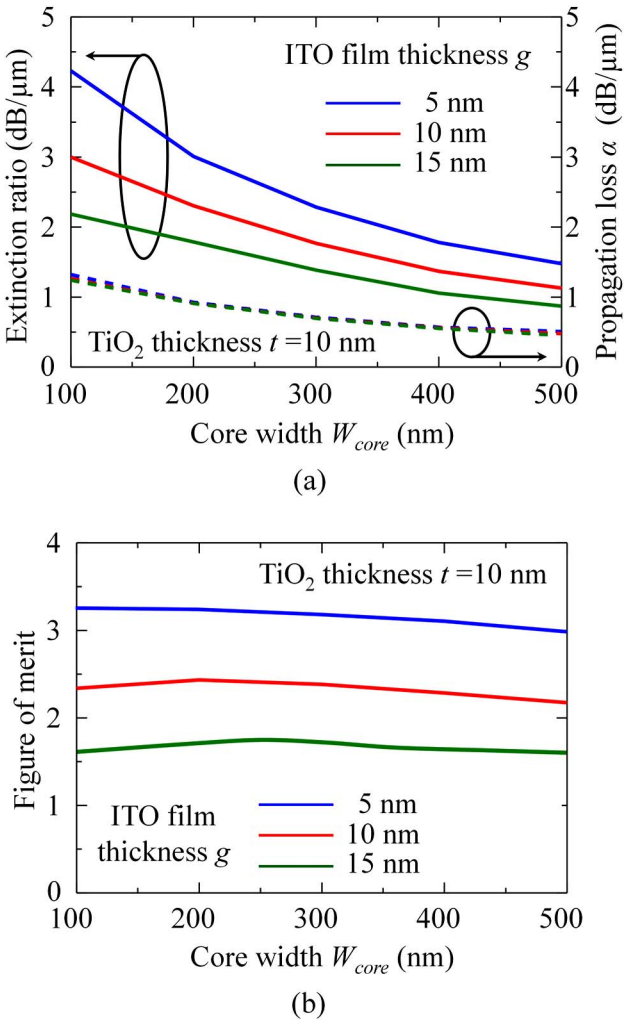

Fig. 7. (a) Calculated extinction ratio and propagation loss without gate bias as a function of W_{core}. (b) Calculated figure of merit as a function of W_{core}.

metallic state at the TiO_2/ITO interface. This increases the light confinement inside the GSPP waveguide and consequently increases the absorption loss in the metal. That is, our device modulates the light intensity by varying the optical confinement near the gate metal.

The extinction ratio and insertion loss (propagation loss at gate voltage = 0 V) can be obtained from the complex refractive index of the waveguide for each GSPP wave state. The extinction ratio and propagation loss as a function of W_{core} are shown in Fig. 7(a), with the ITO thickness as a parameter. An extinction ratio of 4.2 dB/μm was obtained for an ITO thickness of 5 nm and W_{core} = 100 nm. It monotonously decreases with an increase in ITO thickness. This is because the confinement of the GSPP waves becomes weak with an increase in ITO thickness, and consequently the effect of the dielectric–metallic transition of the ITO layer on the GSPP waves also becomes weak. Finally, we calculated the figure of merit defined by the ratio of the extinction ratio and the insertion loss in the off state. Figure 7(b) gives the result as a function of W_{core}. A value of approximately 3 was obtained, with an ITO thickness of 5 nm and a wide range of W_{core} values from 100 to 500 nm.

Table 2. Comparison of Plasmon Modulators in Main Academic Institutions

Group	UC Berkeley[a]	Karlsruhe Institute of Technology[a]	This Work
Papers	[24]	[13,23]	This Work
Material	ITO/silicon	ITO/silicon	ITO/GaInAsP/InP
Extinction ratio (ER)	0.8 dB/μm	2.2 dB/μm	4.2 dB/μm
Off-state propagation loss (α)	−1.0 dB/μm	−8.6 dB/μm	−1.3 dB/μm
Figure of merit (ER/α)	0.8	0.25	3.23
Polarization state	TM	TM	TE

[a]Data reported by UC Berkeley and Karlsruhe Institute of Technology are experimental results.

6. CONCLUSION

We proposed a III–V-based electro-absorption plasmon modulator to construct fully monolithic plasmonic integrated circuits. The device consists of a GSPP waveguide with a FinFET-like gate structure to control the transmission of light. We confirmed the operation of the device with the aid of computer simulation. The extinction ratio was 4.2 dB/μm with a gate voltage swing of 0–5, and the insertion loss was 1.3 dB/μm.

Table 2 compares the performance of our device with that of plasmon modulators developed by other research institutes. Our device can achieve a large extinction ratio and figure of merit. The remarkable advantage of our design is that it is InP-based and operates in the TE mode, unlike other similar devices. This makes our design quite compatible with fully monolithic plasmon integrated circuits.

ACKNOWLEDGMENTS

This work was supported in part by the Ministry of Education, Culture, Sports, Science and Technology (MEXT); JSPS KAKENHI Grant Nos. 24246061, 25420321, and 25709026. One of the authors (T. A.) acknowledges support from the Konica Minolta Science and Technology Foundation.

REFERENCES

1. R. Nagarajan, C. H. Joyner, R. P. Schneider, Jr., J. S. Bostak, T. Butrie, A. G. Dentai, V. G. Dominic, P. W. Evans, M. Kato, M. Kauffman, D. J. H. Lambert, S. K. Mathis, A. Mathur, R. H. Miles, M. L. Mitchell, M. J. Missey, S. Murthy, A. C. Nilsson, F. H. Peters, S. C. Pennypacker, J. L. Pleumeekers, R. A. Salvatore, R. K. Schlenker, R. B. Taylor, H. S. Tsai, M. F. V. Leeuwen, J. Webjorn, M. Ziari, D. Perkins, J. Singh, S. G. Grubb, M. S. Reffle, D. G. Mehuys, F. A. Kish, and D. F. Welch, "Large-scale photonic integrated circuits," IEEE J. Sel. Top. Quantum Electron. **11**, 50–65 (2005).
2. J. J. G. M. van der Tol, Y. S. Oei, U. Khalique, R. Ntzel, and M. K. Smit, "InP-based photonic circuits: comparison of monolithic integration techniques," Prog. Quantum Electron. **34**, 135–172 (2010).
3. L. A. Coldren, S. C. Nicholes, L. Johansson, S. Ristic, R. S. Guzzon, E. J. Norberg, and U. Krishnamachari, "High performance InP-based photonic ICsea tutorial," J. Lightwave Technol. **29**, 554–570 (2011).

4. R. A. Soref and B. R. Bennet, "Electrooptical effects in silicon," IEEE J. Quantum Electron. **23**, 123–129 (1987).
5. R. A. Soref, "Silicon-based optoelectronics," Proc. IEEE **81**, 1687–1706 (1993).
6. B. Analui, D. Guckenberger, D. Kucharski, and A. Narasimha, "A fully integrated 20-Gb/s optoelectronic transceiver implemented in a standard 0.13-μm CMOS SOI technology," IEEE J. Solid-State Circuits **41**, 2945–2955 (2006).
7. S. Assefa, W. M. Green, A. Rylyakov, C. Schow, F. Horst, and Y. Vlasov, "CMOS integrated nanophotonics: enabling technology for exascale computing systems," in *Optical Fiber Communication Conference/National Fiber Optic Engineers Conference*, OSA Technical Digest (CD) (Optical Society of America, 2011), paper OMM6.
8. D. Liang, A. W. Fang, H.-W. Chen, M. N. Sysak, B. R. Koch, E. Lively, O. Raday, Y.-H. Kuo, R. Jones, and J. E. Bowers, "Hybrid silicon evanescent approach to optical interconnects," Appl. Phys. A **95**, 1045–1057 (2009).
9. D. Van Thourhout, T. Spuesens, S. K. Selvaraja, L. Liu, G. Roelkens, R. Kumar, G. Morthier, P. Rojo-Romeo, F. Mandorlo, P. Regreny, O. Raz, C. Kopp, and L. Grenouillet, "Nanophotonic devices for optical interconnect," IEEE J. Sel. Top. Quantum Electron. **16**, 1363–1375 (2010).
10. G. Roelkens, L. Liu, D. Liang, R. Jones, A. Fang, B. Koch, and J. E. Bowers, "III-V/silicon photonics for on-chip and intra-chip optical interconnects," Laser Photon. Rev. **4**, 751–779 (2010).
11. Y. Urino, T. Horikawa, T. Nakamura, and Y. Arakawa, "High density optical interconnects integrated with lasers, optical modulators and photodetectors on a single silicon chip," in *Optical Fiber Communication Conference/National Fiber Optic Engineers Conference*, OSA Technical Digest (online) (Optical Society of America, 2013), paper OM2J.6.
12. E. Ozbay, "Plasmonics: merging photonics and electronics at nanoscale dimensions," Science **311**, 189–193 (2006).
13. A. Melikyan, M. Sommer, A. Muslija, M. Kohl, S. Muehlbrandt, A. Mishra, V. Calzadilla, Y. Justo, J. P. Martínez-Pastor, I. Tomkos, A. Scandurra, D. Van Thourhout, Z. Hens, M. Smit, W. Freude, C. Koos, and J. Leuthold, "Chip-to-chip plasmonic interconnects and the activities of EU project NAVOLCHI," in *Proceedings of the 14th International Conference on Transparent Optical Networks (ICTON)* (IEEE, 2012), paper Th.A5.1.
14. J. T. Kim and S. Park, "The design and analysis of monolithic integration of CMOS-compatible plasmonic waveguides for on-chip electronic-photonic integrated circuits," J. Lightwave Technol. **31**, 2974–2981 (2013).
15. J. Takahara, S. Yamagishi, H. Taki, A. Morimoto, and T. Kobayashi, "Guiding of a one-dimensional optical beam with nanometer diameter," Opt. Lett. **22**, 475–477 (1997).
16. M. T. Hill, "Status and prospects for metallic and plasmonic nano-lasers [Invited]," J. Opt. Soc. Am. B **27**, B36–B44 (2010).
17. R.-M. Ma, R. F. Oulton, V. J. Sorger, G. Bartal, and X. Zhang, "Room-temperature sub-diffraction-limited plasmon laser by total internal reflection," Nat. Mater. **10**, 110–113 (2011).
18. K. Ding, Z. C. Liu, L. J. Yin, M. T. Hill, M. J. H. Marell, P. J. van Veldhoven, R. Nöetzel, and C. Z. Ning, "Room-temperature continuous wave lasing in deep-subwavelength metallic cavities under electrical injection," Phys. Rev. B **85**, 041301 (2012).
19. M. Khajavikhan, A. Simic, M. Katz, J. H. Lee, B. Slutsky, A. Mizrahi, V. Lomakin, and Y. Fainman, "Thresholdless nanoscale coaxial lasers," Nature **482**, 204–207 (2012).
20. L. Tang, S. E. Kocabas, S. Latif, A. K. Okyay, D.-S. Ly-Gagnon, K. C. Saraswat, and D. A. B. Miller, "Nanometre-scale germanium photodetector enhanced by a near infrared dipole antenna," Nat. Photonics **2**, 226–229 (2008).
21. P. Neutens, P. Van Dorpe, I. De Vlaminck, L. Lagae, and G. Borghs, "Electrical detection of confined gap plasmons in metal–insulator–metal waveguides," Nat. Photonics **3**, 283–286 (2009).
22. M. W. Knight, H. Sobhani, P. Nordlander, and N. J. Halas, "Photodetection with active optical antennas," Science **332**, 702–704 (2011).
23. A. Melikyan, N. Lindenmann, S. Walheim, P. M. Leufke, S. Ulrich, J. Ye, P. Vincze, H. Hahn, T. Schimmel, C. Koos, W. Freude, and J. Leuthold, "Surface plasmon polariton absorption modulator," Opt. Express **19**, 8855–8869 (2011).
24. V. J. Sorger, N. D. Lanzillotti-Kimura, R.-M. Ma, and X. Zhang, "Ultra-compact silicon nanophotonic modulator with broadband response," Nanophotonics **1**, 1–6 (2012).
25. J. T. Guske, J. Brown, A. Welsh, and S. Franzen, "Infrared surface plasmon resonance of AZO-Ag-AZO sandwich thin films," Opt. Express **20**, 23215–23226 (2012).
26. V. E. Babicheva, N. Kinsey, G. V. Naik, M. Ferrera, A. V. Lavrinenko, V. M. Shalaev, and A. Boltasseva, "Towards CMOS-compatible nanophotonics: ultra-compact modulators using alternative plasmonic materials," Opt. Express **21**, 27326–27337 (2013).
27. P. I. Rovira and R. W. Collins, "Analysis of specular and textured SnO_2: F films by high speed four-parameter Stokes vector spectroscopy," J. Appl. Phys. **85**, 2015–2025 (1999).
28. S. Brehme, F. Fenske, W. Fuhs, E. Nebauer, M. Poschenrieder, B. Selle, and I. Sieber, "Free-carrier plasma resonance effects and electron transport in reactively sputtered degenerate ZnO:Al films," Thin Solid Films **342**, 167–173 (1999).
29. V. Singh, R. M. Mehra, A. Yoshida, and A. Wakahara, "Doping mechanism in aluminum doped zinc oxide films," J. Appl. Phys. **95**, 3640–3643 (2004).
30. K. Ellmer, "Resistivity of polycrystalline zinc oxide films: current status and physical limit," J. Phys. D **34**, 3097–3108 (2001).
31. T. Pisarkiewicz, K. Zakrzewska, and E. Leja, "Scattering of charge carriers in transparent and conducting thin oxide films with a non-parabolic conduction band," Thin Solid Films **174**, 217–223 (1989).
32. R. F. Oulton, V. J. Sorger, D. A. Genov, D. F. P. Pile, and X. Zhang, "A hybrid plasmonic waveguide for subwavelength confinement and long-range propagation," Nat. Photonics **2**, 496–500 (2008).